

pubs.acs.org/acsapm Article

Multiwavelength Photodetectors Based on an Azobenzene Polymeric Ionic Liquid

Angelique M. Scheuermann, Hiba Wakidi, Alexander T. Lill, Saejin Oh, Luana C. Llanes, Colton A. D'Ambra, Ségolène Antoine, Ming Wang, Michael L. Chabinyc, Thuc-Quyen Nguyen, Javier Read de Alaniz,* and Christopher M. Bates*



Cite This: ACS Appl. Polym. Mater. 2021, 3, 5125-5133



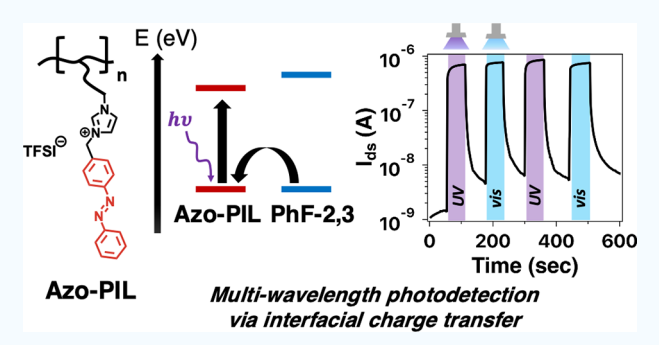
ACCESS

Metrics & More

Article Recommendations

s) Supporting Information

ABSTRACT: Organic photodetectors (OPDs) are a promising class of light-detecting devices that can be created with simple fabrication techniques from a large variety of chemical building blocks. While molecular photoswitches are commonly used to modulate the properties of these devices through reversible isomerization or charge transfer, this responsive behavior is typically limited to a small range of wavelengths. Here, we report the characteristics of multi-wavelength photodetectors using bilayers of a light-responsive azobenzene polymeric ionic liquid (PIL) in conjunction with the semiconducting polymer poly{(4,4-dihexadecyl-4H-cyclopenta[1,2-b:5,4-b'] dithiophene-2,6-diyl)-alt-(2,3-difluoro-1,4-phenylene)} (PhF-2,3). Both ultraviolet (UV) and visible light induce a 10^2 - 10^3



increase in current at a constant voltage within 10 s, which decays immediately when the light is turned off. This light-mediated performance is fatigue-resistant across multiple ON/OFF cycles and can be modulated with wavelengths far into the visible region (660 and 700 nm). Frontier energy level calculations of the light-induced charge carrier density indicate that this light-responsive increase in current is due to photoexcitation and a subsequent charge-transfer process between the azobenzene polymeric ionic liquid and the semiconducting polymer. In summary, the device described in this report exhibits sensing capabilities for multiple wavelengths of light corresponding with the azobenzene absorption profile.

KEYWORDS: photodetector, azobenzene, charge transfer, multiwavelength sensing, polymeric ionic liquid

■ INTRODUCTION

Organic photodetectors (OPDs) have a tunable wavelength response and are compatible with flexible/lightweight form factors. ¹⁻⁴ The chemical versatility of organic semiconducting materials used to fabricate OPDs provides a wide range of accessible absorption profiles and physical properties that are important in various applications. For example, these materials can be deposited over large areas with solution-based methods (e.g., spin-coating, inkjet printing, and roll-to-roll printing) and are processable under ambient (or convenient) conditions. ²⁻⁶

One strategy to create OPDs and other light-responsive devices leverages molecular photoswitches (including spiropyran, azobenzene, and diarylethene), which remotely modify the properties of organic semiconductors in response to light. Among these photoswitches, azobenzenes have been widely studied due to their synthetic accessibility and stable cycling performance. Azobenzenes have been used to modulate the electrical properties of thin-film transistors both under and after illumination when incorporated as the gate insulator or directly in the semiconductor layer. Generally, these effects are related to charge trapping Generally, or photomediated

changes in the azobenzene dipole moment that accompanies *cis—trans* isomerization. ^{16,17}

Despite the appeal of OPD devices containing organic semiconductors and photoswitches, there are two major challenges associated with practical implementation. First, the wavelength range over which they respond to light is typically limited to a narrow region around the absorption profile of the two photoswitch states, e.g., *trans-* and *cis-*azobenzene. Second, there are often processing difficulties in forming thin-film stacks containing organic semiconductors and light-responsive azobenzene-based materials because of their similar solubilities. Here, we overcome these limitations by exploiting azobenzene-containing polymeric ionic liquids (PILs) as efficient materials for multiwavelength detection in OPDs

Received: July 20, 2021 Published: September 14, 2021





Figure 1. Synthesis of Azo-PIL via postpolymerization modification of poly(allyl glycidyl ether). (i) Light-mediated thiol—ene click with pendant alkenes initiated by 2,2-dimethoxy-2-phenylacetophenone (DMPA) in methanol over 2 h at room temperature. (ii) Partial quaternization of imidazole side chains with 1-(4-(bromomethyl)phenyl)-2-phenyldiazene in 1:1 methanol/acetonitrile at 100 °C for 15 h. (iii) Ion exchange with lithium bis(trifluoromethanesulfonyl)imide (LiTFSI) in 20% water in methanol at 50 °C for 18 h.

when used as a gate layer with the semiconducting p-type polymer poly{(4,4-dihexadecyl-4H-cyclopenta[1,2-b:5,4-b']dithiophene-2,6-diyl)-alt-(2,3-difluoro-1,4-phenylene)} (PhF-2,3). PILs are advantageous as light-responsive gate materials because they exhibit good solubility in polar solvents, which allows for direct deposition via spin-coating onto less polar semiconducting conjugated polymers. Moreover, PILs retain the advantageous qualities of ionic liquids (ILs) such as good thermal stability and low volatility while providing tunable mechanical and physical properties through synthesis. 18 Our photoswitch-based photodetector platform shows an increase in photocurrent over 2-to-3 orders of magnitude when exposed to different wavelengths of light, as well as an attenuated response across the visible spectrum. These multiwavelength sensing capabilities expand the applicability of photoswitches and PILs in flexible, solution-processable devices for broadband light detection.

■ RESULTS AND DISCUSSION

Design and Synthesis of a Photoresponsive PIL with Pendant Azobenzene Groups. We sought to develop a PIL-containing photoswitch as a light-responsive unit with high solubility in orthogonal solvents to the organic semiconducting polymer PhF-2,3. PhF-2,3 is a donor—acceptortype semiconducting polymer based on 4,4-dihexadecyl-4*H*-cyclopenta[1,2-*b*:5,4]dithiophene (CDT) and 2,3-difluorophenylene (2,3-DFPh) that was chosen for its high hole mobility. The electron-withdrawing property of 2,3-DFPh is relatively weak in comparison with conventional acceptor units, which results in a higher-lying LUMO level that provides a sufficient energetic barrier for minimizing electron injection from gold, thereby facilitating unipolar hole transport in the semiconductor.

For the light-responsive PIL layer, we designed a polymer with covalently attached azobenzene units and, importantly, fixed charge groups that would solubilize the material in polar solvents for direct deposition onto PhF-2,3 (which is soluble in nonpolar solvents). Poly(ethylene oxide) was chosen as the PIL polymer backbone because it is a synthetically accessible and soluble scaffold that has a low $T_{\rm g}$ to avoid aggregation of the azobenzene chromophore, which could lead to nonuniform

and irreversible performance in devices. 13,17 A poly(ethylene oxide) homopolymer with side chains containing neutral imidazoles ($T_g = -20$ °C) was synthesized as the PIL precursor through a thiol—ene click reaction according to previously reported literature. ²¹ Postpolymerization modification of this PIL precursor by partial quaternization of imidazoles with 1-(4-(bromomethyl)phenyl)-2-phenyldiazene²² yielded a photoresponsive azobenzene PIL (Figure 1). This simple synthetic approach installs the charged imidazolium group and covalently bound azobenzene in tandem with stoichiometric control over the level of functionalization. The extent of quaternization as measured by ¹H nuclear magnetic resonance (NMR) (details shown in the Supporting Information) was 37 mol %, which agrees well with the target of 40 mol % azobenzene-IL incorporation. This concentration of PIL and azobenzene represents a suitable balance between ionicity for solubility without making the material too optically dense for effective light penetration. 23,24 The bromide anion was then exchanged for bis(trifluoromethanesulfonyl)imide (TFSI) (Figure S5) via ion metathesis to form a PIL denoted Azo-PIL ($T_g = -11$ °C). The larger, more diffuse TFSI anion improves solubility in organic solvents and reduces the $T_{\rm g}$ compared to other possible PIL counterions. 25,26

Fatigue-Resistant trans-cis Isomerization. Upon covalent attachment to Azo-PIL via side-chain imidazoles, the isomerization of azobenzene in the solid state was photochemically characterized by UV-vis spectroscopy (Figure 2a). Azo-PIL in acetone was spin-coated onto quartz substrates to prepare 400 nm thin-film samples. The penetration depth of light in a thin film can be calculated as $l = \alpha^{-1}$, where l is the penetration depth and α is the attenuation coefficient at a specific wavelength of light (Table S1).²⁷ At the wavelengths of interest for azobenzene (365 and 470 nm), 10 the penetration depth is roughly 430 and 620 nm, respectively, based on 37% azobenzene in the PIL. Thus, at the film thicknesses used in UV-vis experiments, some incident light will be transmitted through the film. We first irradiated these samples with 365 nm light (80 mW cm⁻²) to induce trans-to-cis isomerization. In the UV-vis spectrum of Azo-PIL (Figure 2b), isomerization to the cis isomer corresponds with a decrease in the λ_{max} at 323 nm, largely associated with the $\pi \to \pi^*$ transition of trans-

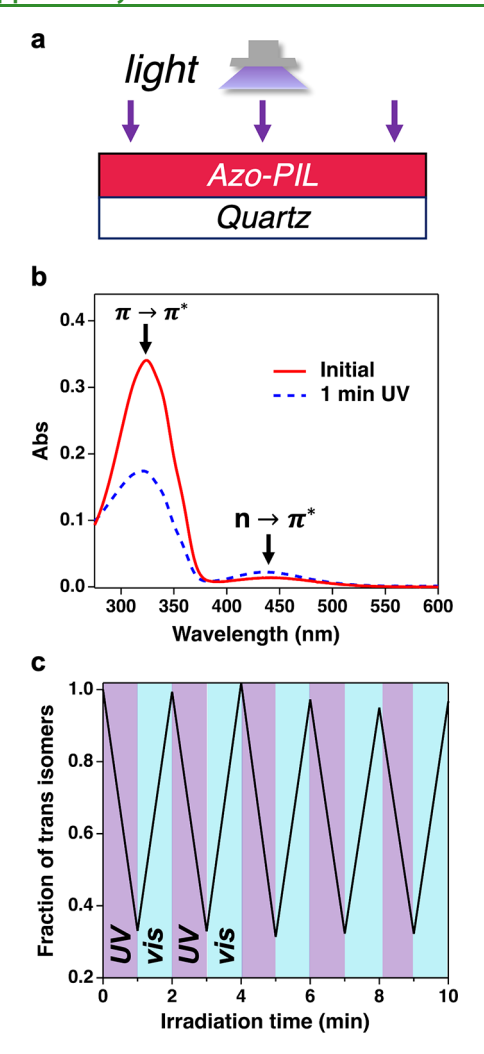


Figure 2. UV—vis studies of Azo-PIL thin films were conducted on quartz. (a) Schematic of the irradiation setup. (b) UV—vis spectra of thin-film Azo-PIL before (solid red trace) and after (dashed blue trace) exposure to 365 nm irradiation for 1 min. (c) Fraction of the *trans* azobenzene isomer during multiple irradiation cycles with UV (365 nm, 80 mW cm⁻²) and visible (470 nm, 200 mW cm⁻²) light.

azobenzene. The concomitant increase in $\lambda_{\rm max}$ at 430 nm is related to the n $\rightarrow \pi^*$ transition of cis-azobenzene, which was observed after 1 min of irradiation with 365 nm light. Subsequent irradiation with 470 nm light (200 mW cm⁻²) for 1 min resulted in back isomerization from cis to trans. Prolonged irradiation with either 365 or 470 nm did not induce further changes in the UV—vis spectrum of Azo-PIL, indicating that 1 min of irradiation is sufficient to reach a photostationary state (PSS) (Figures S8 and S9).

The *cis-trans* ratio at the photostationary state was quantified by UV-vis spectroscopy and ¹H NMR by extrapolating *trans* and *cis* extinction coefficients (Table S2 and Figure S10, Supporting Information). ²⁸ Calculated by this method, the PSS corresponds with 67% *cis* under 365 nm light. Partially overlapping absorbances of *trans* and *cis* states around 365 nm, which presumably results from the proximity of azobenzene to an electron-withdrawing imidazolium, contribute to the modest *cis* content of the PSS; ²³ in comparison with other polymers that are covalently conjugated to an azobenzene unit, we observe a slightly lower percentage of *cis* isomer in Azo-PIL at the PSS (typically ~89–95% *cis* form is observed after exposure to UV light). ^{29–31} However, the *trans*-to-*cis* ratio under UV light in Azo-PIL is consistent with the switching efficiency of a previously reported small-molecule azobenzene ionic liquid. ²²

Next, we performed cyclic irradiation UV-vis studies of Azo-PIL under 365 and 470 nm light to mimic the irradiation conditions used in devices. Exposing Azo-PIL films to alternating 365 and 470 nm light demonstrates the excellent reversibility of the *cis-trans* isomerization with a negligible decay in performance (Figure 2c). Once deposited on the semiconducting polymer PhF-2,3, Azo-PIL preserves its reversible isomerization characteristics with a decreased absorbance in the $\pi \to \pi^*$ transition at 323 nm upon UV light irradiation and a return to the original UV-vis spectrum with visible light (Figure S11).

Multi-Wavelength-Stimulated Increase in Photocurrent Driven by Absorption of Azobenzene. With the reversible photochemical properties of Azo-PIL confirmed by UV—vis studies, both two- and three-terminal lateral organic bilayer photodetectors were fabricated to investigate the light-induced device response and associated molecular mechanism.

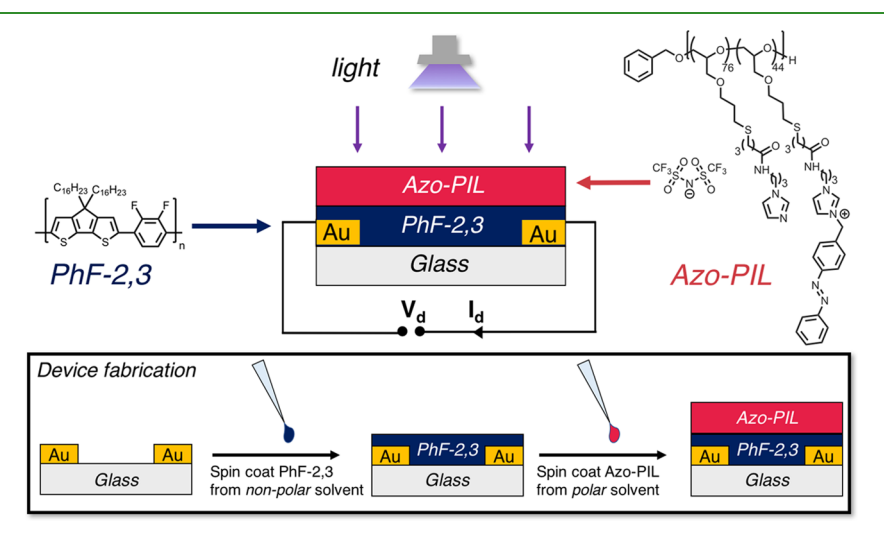


Figure 3. Schematic of the two-terminal photodetector device fabrication by spin-coating Azo-PIL directly onto the semiconducting polymer PhF-2,3 on a glass substrate (previously passivated with *n*-decyltrichlorosilane (DTS)).

Azo-PIL and PhF-2,3 were introduced as photoactive and semiconducting layers, respectively. Due to the orthogonal solubilities of Azo-PIL and PhF-2,3, Azo-PIL could be spin-coated onto PhF-2,3 without the need for an intermediate layer (Figure 3). Details about the fabrication methods for the devices are further described in the Supporting Information.

The response produced in these bilayer devices under irradiation was studied by monitoring the drain current as a function of time under exposure to 365 and 470 nm light. When the photodetector was initially illuminated with 365 nm light (80 mW cm⁻²), a 600-fold increase over 3 orders of magnitude in drain current was observed with a rise time of 10 s (Figure 4a).

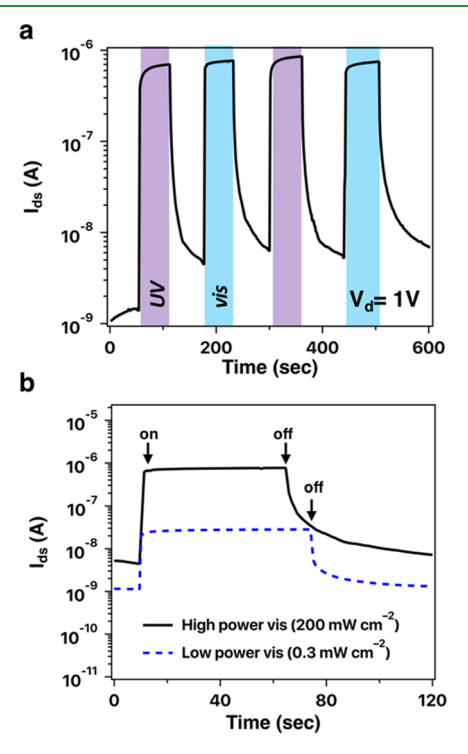


Figure 4. Time-dependent current of the two-terminal device in response to (a) alternating UV (365 nm, 80 mW cm $^{-2}$) and visible (470 nm, 200 mW cm $^{-2}$) light, and (b) high (200 mW cm $^{-2}$) and low (0.3 mW cm $^{-2}$) power visible light (470 nm).

After approximately a rise time of 50 s, saturation at 99% of the final current was reached. Notably, a 90% relaxation of the

current was observed within a fall time of 5 s when the 365 nm light was shut OFF, eventually resulting in a 99% decrease in current after a fall time of 70 s in the dark. To test the response to light within a timespan of minutes, the device was subsequently irradiated with 470 nm light (200 mW cm⁻²), eliciting an increase over 2 orders of magnitude to the same maximum value in current. In following irradiation cycles, the increase in current and decay with 470 nm is nearly identical to the response under 365 nm light. This fast ON–OFF performance is maintained upon repeated cycling between 365 and 470 nm light (Figure 4a), a performance that is within the range of 14,15 or exceeds 7,16 other photochromism-based devices.

As the increase in current was shown to be consistent with multiple cycles of irradiation with 365 and 470 nm light, the sensitivity of the device was then examined by comparing the effect of incident power at 470 nm (0.3 and 200 mW cm⁻²) (Figure 4b). Bias-stress measurements of the two-terminal device under 470 nm at 0.3 mW cm⁻² show an increase in current of approximately 1 order of magnitude, smaller than the 3 orders of magnitude increase observed under higher power (200 mW cm⁻²). Although the irradiation with our high-powered 470 nm light-emitting diode (LED) (200 mW cm⁻²) is 670 times higher than that of the low-powered LED (0.3 mW cm⁻²), the current increase observed is only 25 times larger. Additionally, a responsivity of 0.23 A W^{-1} and an external quantum efficiency (EQE) of 59% was calculated at this low-powered 470 nm, comparable to what is found in other planar heterojunction OPDs (Table S3, Supporting Information). This nonlinear dependence on power density reveals the limits of the current increase, sensitivity, and performance of this device as an OPD.

Encouraged by these results, we next sought to determine if the Azo-PIL device would be applicable as a broadband photodetector through exposure to different wavelengths of light beyond the Azo-PIL wavelengths of maximum absorption. We selected three wavelengths of light with three different photon fluxes. Specifically, the device response under 470 nm was compared to 660 and 700 nm wavelengths, which are lower energy than the $\pi \to \pi^*$ and $n \to \pi^*$ transitions of trans-Azo-PIL and are near the absorption edge of PhF-2,3 (Figure 5b). Bias-stress measurements of the two-terminal photodetector under lower power 470 nm light (0.32 mW cm⁻²; 7.7 × 10^{14} photons s⁻¹ cm⁻²) show an increase in current of approximately 1 order of magnitude (Figure 5a). In comparison, the current increase under a 660 nm LED (2.1

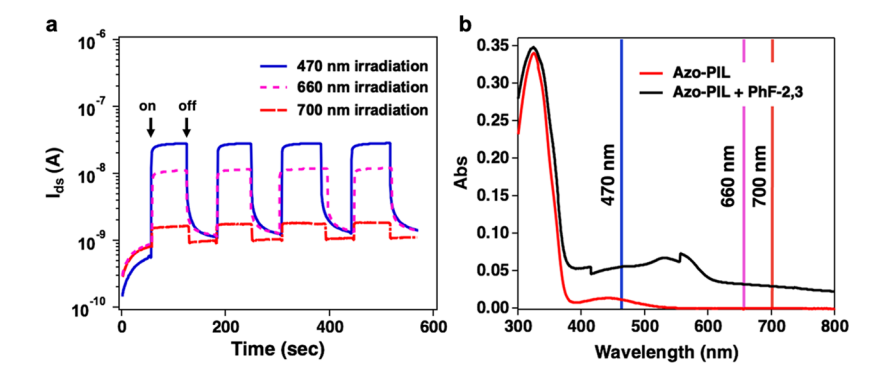


Figure 5. (a) Time-dependent current of the two-terminal device under irradiation with three wavelengths of light. (b) UV—vis spectrum of *trans*-Azo-PIL and trans-Azo-PIL + PhF-2,3 on quartz with the wavelengths of irradiation from (a) highlighted. Panel (b) shows 470 nm has absorption from both Azo-PIL and PhF-2,3, whereas PhF-2,3 contributes to the majority of the absorption at 660 and 700 nm.

mW cm⁻²; 6.9×10^{15} photons s⁻¹ cm⁻²) is 37% of the current increase seen with 470 nm light, despite a higher photon flux. With 700 nm light (1.5 mW cm⁻²; 5.2×10^{15} photons s⁻¹ cm⁻²), the increase in drain current under constant bias stress was 3% of the increase in current seen with 470 nm light (Figure 5a). For all three wavelengths of light with differing photon fluxes, we see an increase in current, demonstrating the capability of this device to detect light of various wavelengths and corresponding energies.

To evaluate if the increase in photocurrent was dependent on the concentration of trans or cis isomers in the Azo-PIL layer, the light response of bilayers was compared in the presence and absence of the *trans* \rightarrow *cis* isomerization. A threeterminal device where the bilayer was formed on an SiO₂ dielectric with a doped silicon bottom gate provided a means to modulate the number of carriers in Ph-2,3 at the SiO₂ interface and into the bulk by application of a gate bias. Measurements were performed in the saturation regime (V_D = -80 V) of the device under irradiation with 365 and 470 nm light. The devices were first kept in the dark to ensure that the Azo-PIL layer was initially in the trans form. These threeterminal Azo-PIL devices were then irradiated with 365 or 470 nm light. Note that little $trans \rightarrow cis$ isomerization is observed when the Azo-PIL film in the trans form is illuminated with 470 nm LED light (Figure S12). As expected from Figure 4a, an increase in current at all voltages was observed with 365 nm light (Figure 6). Notably, a similar shift in the transfer curve

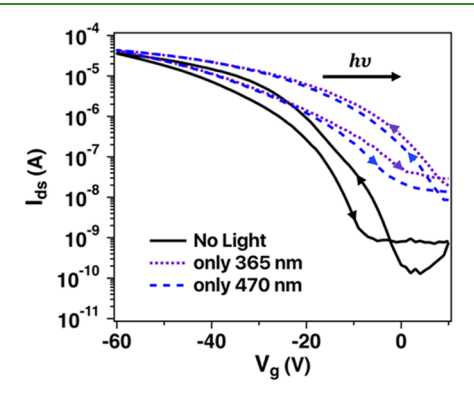


Figure 6. Transfer characteristics of the three-terminal Azo-PIL device under dark conditions (trans form), after 365 nm irradiation (*trans* \rightarrow *cis* isomerization), and after 470 nm irradiation (still in the trans form).

was observed with 470 nm illumination that corresponds with minimal $trans \rightarrow cis$ isomerization, presumably due to minor absorbance from the $n \rightarrow \pi^*$ transition of trans-azobenzene.

Mechanism. The increase in current observed with UV light could be consistent with either the isomerization of azobenzene, which yields a change in dipole moment 16,1716,17 or a light-induced charge-transfer mechanism. With Azo-PIL, evidence suggests charge transfer between the Azo-PIL and PhF-2,3 semiconducting layers is responsible for the current increase.

First, as shown above in Figure 6, molecules that remain in the *trans* configuration still increase device current when illuminated. Second, a change in dipole driving the conductivity does not fully explain why the current increase is the same with both 365 and 470 nm light sources; as shown in Figure 2, Azo-PIL undergoes a reversible isomerization with 365 and 470 nm light. If the change in dipole controlled the

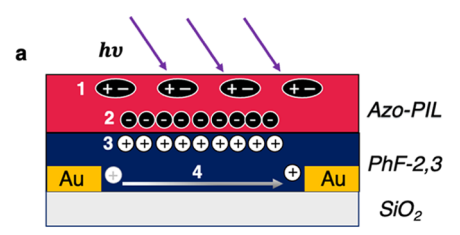
increase in current, a *cis—trans* isomerization would decrease the current as *cis* reverts back to *trans* if molecular dipole effects were at play, suggesting that charge transfer is the mechanism in the Azo-PIL device.

Our hypothesis of charge transfer is further supported by the higher OFF current under 365 and 470 nm light for the reverse scan of the transfer curve. Full current recovery was not observed during the reverse bias scans, which can be attributed to incomplete charge depletion in the bulk PhF-2,3 layer. The trapped charges in the PhF-2,3 layer are believed to keep the device ON during the reverse bias scan above 0 V, which indicates that charge transfer occurs at the Azo-PIL and PhF-2,3 interface.

Furthermore, this device shows the largest increases in current for the wavelengths of light associated with Azo-PIL absorbance. As shown in Figure 5, we observed a difference in the increase in photocurrent under 470 nm light, associated with Azo-PIL, and that under 660 and 700 nm light, outside of the Azo-PIL absorbance spectrum. Although the respective photon fluxes of light with 660 nm $(6.9 \times 10^{15} \text{ photons s}^{-1})$ cm⁻²) and 700 nm (5.2 \times 10¹⁵ photons s⁻¹ cm⁻²) are larger than that of the 470 nm LED (7.7 \times 10¹⁴ photons s⁻¹ cm⁻²) used in this experiment, a smaller current increase was observed, resulting in smaller responsivities and external quantum efficiency (EQEs) at these longer wavelengths (Table S3, Supporting Information). Additionally, PhF-2,3 absorbs at 660 and 700 nm and shows a small amount of charge carriers generated compared to the wavelengths where Azo-PIL absorbs, implying formation of the exciton in the Azo-PIL layer (Table S1, Supporting Information).

Finally, in the absence of the Azo-PIL layer, the device containing only PhF-2,3 shows minimal increases in current with irradiation of multiple wavelengths of light despite the fact that PhF-2,3 does show some absorbance at 470, 660, and 700 nm in the UV—vis spectrum¹⁹ (Figures S13 and S14). Taken altogether, these results strongly support that the device response is driven by Azo-PIL absorption and subsequent charge transfer with the PhF-2,3 semiconductor.

Frontier energy levels of PhF-2,3 and Azo-PIL were determined experimentally by cyclic voltammetry to further support the interfacial charge-transfer mechanism (Figure S15). The highest-occupied molecular orbital (HOMO) and lowest-unoccupied molecular orbital (LUMO) of Azo-PIL were calculated using a ferrocene reference (4.8 eV), yielding a HOMO energy of -5.3 eV and LUMO energy of -4.1 eV. We believe that these HOMO and LUMO levels are due to the azobenzene units on Azo-PIL as the corresponding oxidation and reduction peaks used for HOMO-LUMO determination are present in Azo-PIL but are absent from the unfunctionalized imidazole homopolymer (Figures S15 and S16, Supporting Information). The HOMO and LUMO energies of PhF-2,3 have previously been reported as -5.3 and -3.3 eV, respectively. 19 With the similar HOMO levels of Azo-PIL and PhF-2,3 coupled with the fact that PhF-2,3 does not absorb light at 365 nm, 19 it is plausible that the generation of an exciton in the Azo-PIL layer would allow for hole transfer from the HOMO of Azo-PIL to the HOMO of PhF-2,3, thereby reducing azobenzene in the Azo-PIL layer and yielding holes in PhF-2,3 (Figure 7). This photoinduced interfacial hole transfer increases the hole current within the semiconductor, even with multiple wavelengths of light. In addition, the quick decay of current in the absence of light is consistent with recombination between carriers near the interface of Azo-PIL and PhF-2,3



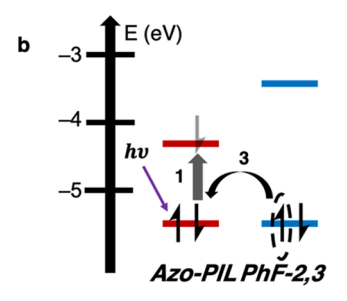


Figure 7. Schematic of the charge transport mechanism as depicted with (a) an interfacial diagram and (b) frontier energy levels. When the device is illuminated with either 365 or 470 nm light, an electron in Azo-PIL is promoted from the low-lying doubly occupied HOMO to the LUMO, generating excitons in the PIL layer (step 1). These excitons diffuse throughout the PIL gate layer to the interface (step 2, not depicted in (b)), stimulating electron transfer from the doubly occupied HOMO of PhF-2,3 to the now singly occupied HOMO of azobenzene and creating holes in the semiconducting layer (step 3). The generation of holes in the semiconducting PhF-2,3 layer then allows for the lateral flow of electrons (step 4, not depicted in (b)), resulting in an increase in current under multiple wavelengths of light.

layers. This decay that begins as soon as the light is turned OFF contrasts with the behavior of past devices, which exploit azobenzene charge transfer; typically, slow decay rates on the order of minutes to hours after UV irradiation are observed due to sluggish hole recombination between the semiconducting polymer and azobenzene additive, maintaining a metastable ON state. ^{11,14,15} In the Azo-PIL device described here, the reduced azobenzene in the Azo-PIL layer can readily transfer an electron back to holes in PhF-2,3 resulting in fast current decay.

To further rationalize the interfacial charge-transfer mechanism between Azo-PIL and PhF-2,3, measurements from two-and three-terminal devices were used to estimate the surface carrier number density. For the two-terminal device, a model for the charge-transfer mechanism was used, and the resulting estimated photogenerated carrier number density was compared to the carrier number density estimated for the three-terminal device. The agreement between these numbers would further support the proposed photoinduced interfacial charge-transfer mechanism.

For the two-terminal device, the expected charge carrier number density can be extracted from the observed current increase, assuming that the current increase is solely due to photoinduced charge transfer at the interface of the two polymers. The photogenerated current $(J_{\rm photo})$ of a two-terminal, lateral organic bilayer heterojunction photoconductor can be described by eq $1^{32,33}$

$$J_{\text{photo}} = qn(\mu_{\text{n}} + \mu_{\text{p}})E \tag{1}$$

where q is the electric charge, n is the charge carrier density, E is the applied electric field, and $\mu_{\rm n}$ and $\mu_{\rm p}$ are the electron and hole mobilities, respectively, such that $\mu_{\rm p}=1.1~{\rm cm^2~V^{-1}~s^{-1}}$ (ref

20) and $\mu_{\rm p}\gg\mu_{\rm n}$. With a current increase of 0.44 $\mu{\rm A}$, the surface photogenerated carrier number density is estimated to be 3×10^{11} carriers cm⁻². To further validate the application of a two-terminal photoconductor model to our system, the carrier number density for the three-terminal device was estimated from the transfer curve in Figure 6. If the values of carrier number density from the two-terminal photoconductor model and calculations based on data from the three-terminal device match, this would support the hypothesis that the current increase is due to photoexcitation of Azo-PIL followed by interfacial charge transfer. The capacitance of the gate (~4 pF) was estimated from the capacitance per unit area of 300 nm thick Si (10.5 nF cm⁻²) and the area of the channel (40 $\mu m \times 1000 \ \mu m$). By assuming that the applied voltage is equal to the shift in the threshold voltage (30 V), the accumulated charge was calculated to be 1.2×10^{-10} coulombs. The carrier number density from the three-terminal device is estimated to be 2×10^{12} carriers cm⁻². A small difference in respective calculated carrier density values can be attributed to an overestimation of the hole mobility in the calculations pertaining to the two-terminal device. This difference can also be due to limitations in exciton diffusion and deviations in the PIL photoluminescence efficiency from 100%, which is seen with both the two-terminal and three-terminal devices. As the value calculated for carrier density of the three-terminal device is within 1 order of magnitude to that of the twoterminal photoconductor model, this finding supports the proposed charge-transfer mechanism and the validity of using this model.³³

Since the photoconductor model is applicable to this system, it can be used to estimate the charge carrier lifetime by extending eq 1 as follows³³

$$J_{\text{photo}} = q\eta \Phi \frac{L}{d} \tau \left(\frac{1}{t_{\text{n}}} + \frac{1}{t_{\text{p}}} \right)$$
 (2)

where η is the photoluminescence efficiency, Φ is the photon flux per unit area, L is the channel length, d is the device thickness, τ is the carrier lifetime, and $t_{\rm n}$ and $t_{\rm p}$ are the transit times of electron and holes, respectively. With the known surface power density of both light sources at each wavelength, the device geometry, and the photon flux attenuated by the Azo-PIL layer, the carrier lifetime (τ) of PhF-2,3 at both wavelengths was extracted and found to be in the microsecond range (details shown in Table S1). These results assume the photoluminescence efficiency to be around \sim 0.05, which is typical for organic semiconducting polymers. Along with the matching frontier energy levels, this analysis leads us to the conclusion that charge transfer occurs at the interface of Azo-PIL and PhF-2,3 and induces a current increase at operating wavelengths across the UV and visible spectrum.

In comparison to other light-responsive devices made with azobenzene as a photoresponsive motif, the performance of the Azo-PIL device described here performs well in terms of minimal decay over multiple cycles and fast response times. Our report also explicitly shows that the $trans \rightarrow cis$ does not have a large effect on the interfacial charge-transfer capabilities of azobenzene as demonstrated by the same increase in current with both 365 ($trans \rightarrow cis$) and 470 nm ($cis \rightarrow trans$) light excitation. In general, larger light-induced increases in current are observed with the azobenzene devices that report operation via charge transfer as opposed to a change in dipole, consistent with the 2–3 orders of magnitude

increase in current observed herein. ^{12,14–16} Although there are examples of larger increases in current, for example, over 6 orders of magnitude in devices that include azobenzene as a charge trap, the application of a large negative gate voltage or irradiation with another wavelength of light was required to cause the current to return to its initial state. ^{12,14,15} In contrast, our device shows an immediate decrease in current in the absence of a light source. However, both devices hold importance in the application of photochromic devices, with previous literature examples more useful as writing/erasing photomemory devices and the Azo-PIL device described here applicable as a light sensor. As a photodetector, our device senses longer wavelengths of light than are common in other photochromic devices.

CONCLUSIONS

In conclusion, we have reported the fabrication of a photodetector that functions via charge transfer between an azobenzene PIL layer and a p-type semiconducting polymer. The Azo-PIL layer was designed to have complementary solubility to the semiconducting polymer, PhF-2,3, which facilitates device fabrication by spin-coating. The Azo-PIL was shown to have a reversible $trans \rightarrow cis$ isomerization through UV-vis spectroscopy under 365 and 470 nm irradiation. However, once incorporated into devices, an increase in current was observed with both wavelengths of light, indicating that the response is surprisingly not due to the reversible trans \rightarrow cis isomerization of azobenzene. Instead, we conclude that charge transfer occurs at the interface of Azo-PIL and PhF-2,3 layers as evidenced by cyclic voltammetry (CV) measurements and supporting calculations. This charge-transfer mechanism results in a fast current response because the HOMO energy levels of Azo-PIL and PhF-2,3 are nearly equivalent. This report reinforces the importance of tailoring materials for contemporary applications, which can increase the processability and performance of advanced devices.

ASSOCIATED CONTENT

Supporting Information

The Supporting Information is available free of charge at https://pubs.acs.org/doi/10.1021/acsapm.1c00884.

Synthetic procedures, characterization (¹H and ¹⁹F NMR, UV-vis), spin-coating procedures, device fabrication, carrier transit and photoluminescence values, thermal analysis (DSC), additional bias-stress measurements, and cyclic voltammetry measurements (PDF)

AUTHOR INFORMATION

Corresponding Authors

Javier Read de Alaniz — Department of Chemistry and Biochemistry, University of California, Santa Barbara, California 93106, United States; Materials Research Laboratory, University of California, Santa Barbara, California 93106, United States; ⊚ orcid.org/0000-0003-2770-9477; Email: javier@chem.ucsb.edu

Christopher M. Bates — Department of Chemistry and Biochemistry, University of California, Santa Barbara, California 93106, United States; Materials Department University of California, Santa Barbara, California 93106, United States; Materials Research Laboratory and Department of Chemical Engineering, University of California, Santa Barbara, California 93106, United States; orcid.org/0000-0002-1598-794X; Email: cbates@ucsb.edu

Authors

Angelique M. Scheuermann – Department of Chemistry and Biochemistry, University of California, Santa Barbara, California 93106, United States

Hiba Wakidi – Department of Chemistry and Biochemistry, University of California, Santa Barbara, California 93106, United States

Alexander T. Lill – Department of Chemistry and Biochemistry, University of California, Santa Barbara, California 93106, United States

Saejin Oh – Department of Chemistry and Biochemistry, University of California, Santa Barbara, California 93106, United States

Luana C. Llanes – Department of Chemistry and Biochemistry, University of California, Santa Barbara, California 93106, United States

Colton A. D'Ambra – Department of Chemistry and Biochemistry, University of California, Santa Barbara, California 93106, United States

Ségolène Antoine – Materials Research Laboratory, University of California, Santa Barbara, California 93106, United States

Ming Wang — Center for Advanced Low-Dimension Materials, Donghua University, Shanghai 200051, China

Michael L. Chabinyc – Materials Department University of California, Santa Barbara, California 93106, United States; orcid.org/0000-0003-4641-3508

Thuc-Quyen Nguyen — Department of Chemistry and Biochemistry, University of California, Santa Barbara, California 93106, United States; Center for Polymers and Organic Solids, University of California, Santa Barbara, California 93106, United States; orcid.org/0000-0002-8364-7517

Complete contact information is available at: https://pubs.acs.org/10.1021/acsapm.1c00884

Author Contributions

A.M.S., M.L.C., T.-Q.N., J.R., and C.M.B. designed materials. A.M.S., S.A., and M.W. synthesized materials. A.M.S, C.A.D., and H.W. characterized materials. H.W. and A.T.L. fabricated devices and carried out device measurements. H.W., A.T.L., and S.O. calculated carrier transit and photoluminescence values. L.C.L. completed cyclic voltammetry measurements. A.M.S., J.R., and C.M.B. wrote the paper.

Funding

This work was supported by the UC Santa Barbara Materials Research Science and Engineering Center (MRSEC) Program of the National Science Foundation under Award No. DMR 1720256 (IRG-2). A.M.S. gratefully acknowledges the National Science Foundation Graduate Research Fellowship Program. Any opinions, findings, and conclusions or recommendations expressed in this material are those of the authors and do not necessarily reflect the views of the National Science Foundation.

Notes

The authors declare no competing financial interest.

ACKNOWLEDGMENTS

The research reported here made use of shared facilities of the UC Santa Barbara Materials Research Science and Engineering Center (MRESC, NSF DMR 1720256), a member of the Materials Research Facilities Network (www.mrfn.org). This work utilized NMR instruments supported by the National Science Foundation under award No. MRI-1920299.

REFERENCES

- (1) Natali, D.; Caironi, M. Organic Photodetectors. In *Photodetectors*; Elsevier, 2016; pp 195–254.
- (2) Ren, H.; Chen, J.; Li, Y.; Tang, J. Recent Progress in Organic Photodetectors and Their Applications. *Adv. Sci.* **2021**, *8*, No. 2002418.
- (3) Simone, G.; Dyson, M. J.; Meskers, S. C. J.; Janssen, R. A. J.; Gelinck, G. H. Organic Photodetectors and Their Application in Large Area and Flexible Image Sensors: The Role of Dark Current. *Adv. Funct. Mater.* **2020**, *30*, No. 1904205.
- (4) Xu, Y.; Lin, Q. Photodetectors Based on Solution-Processable Semiconductors: Recent Advances and Perspectives. *Appl. Phys. Rev.* **2020**, *7*, No. 011315.
- (5) Moonen, P. F.; Yakimets, I.; Huskens, J. Fabrication of Transistors on Flexible Substrates: From Mass-Printing to High-Resolution Alternative Lithography Strategies. *Adv. Mater.* **2012**, *24*, 5526–5541.
- (6) Gelinck, G.; Heremans, P.; Nomoto, K.; Anthopoulos, T. D. Organic Transistors in Optical Displays and Microelectronic Applications. *Adv. Mater.* **2010**, *22*, 3778–3798.
- (7) Xu, C.; Zhang, J.; Xu, W.; Tian, H. Multifunctional Organic Field Effect Transistors Constructed with Photochromic Molecules. *Mater. Chem. Front.* **2021**, *5*, 1060–1075.
- (8) Tian, J.; Liu, Z.; Jiang, W.; Shi, D.; Chen, L.; Zhang, X.; Zhang, G.; Di, C.; Zhang, D. A Conjugated Polymer Containing Arylazopyrazole Units in the Side Chains for Field-Effect Transistors Optically Tunable by Near Infra-Red Light. *Angew. Chem., Int. Ed.* **2020**, *59*, 13844–13851.
- (9) Tian, J.; Liu, Z.; Wu, C.; Jiang, W.; Chen, L.; Shi, D.; Zhang, X.; Zhang, G.; Zhang, D. Simultaneous Incorporation of Two Types of Azo-Groups in the Side Chains of a Conjugated D—A Polymer for Logic Control of the Semiconducting Performance by Light Irradiation. *Adv. Mater.* **2021**, *33*, No. 2005613.
- (10) Bandara, H. M. D.; Burdette, S. C. Photoisomerization in Different Classes of Azobenzene. *Chem. Soc. Rev.* **2012**, *41*, 1809–1825
- (11) Tseng, C.-W.; Huang, D.-C.; Tao, Y.-T. Electric Bistability Induced by Incorporating Self-Assembled Monolayers/Aggregated Clusters of Azobenzene Derivatives in Pentacene-Based Thin-Film Transistors. ACS Appl. Mater. Interfaces 2012, 4, 5483—5491.
- (12) Peimyoo, N.; Li, J.; Shang, J.; Shen, X.; Qiu, C.; Xie, L.; Huang, W.; Yu, T. Photocontrolled Molecular Structural Transition and Doping in Graphene. ACS Nano 2012, 6, 8878–8886.
- (13) Raimondo, C.; Crivillers, N.; Reinders, F.; Sander, F.; Mayor, M.; Samori, P. Optically Switchable Organic Field-Effect Transistors Based on Photoresponsive Gold Nanoparticles Blended with Poly(3-Hexylthiophene). *Proc. Natl. Acad. Sci. U.S.A* **2012**, *109*, 12375–12380.
- (14) Smithson, C. S.; Wu, Y.; Wigglesworth, T.; Zhu, S. A More Than Six Orders of Magnitude UV-Responsive Organic Field-Effect Transistor Utilizing a Benzothiophene Semiconductor and Disperse Red 1 for Enhanced Charge Separation. *Adv. Mater.* **2015**, *27*, 228–233.
- (15) Smithson, C. S.; Ljubic, D.; Wu, Y.; Zhu, S. The Effect of Azobenzene Derivatives on UV-Responsive Organic Thin-Film Transistors with a 2,7-Dipentylbenzo[b]Benzo[4,5]Thieno[2,3-d]-Thiophene Semiconductor. J. Mater. Chem. C 2015, 3, 8090–8096.
- (16) Lee, K. E.; Lee, J. U.; Seong, D. G.; Um, M.-K.; Lee, W. Highly Sensitive Ultraviolet Light Sensor Based on Photoactive Organic Gate

- Dielectrics with an Azobenzene Derivative. J. Phys. Chem. C 2016, 120, 23172–23179.
- (17) Tian, J.; Fu, L.; Liu, Z.; Geng, H.; Sun, Y.; Lin, G.; Zhang, X.; Zhang, G.; Zhang, D. Optically Tunable Field Effect Transistors with Conjugated Polymer Entailing Azobenzene Groups in the Side Chains. *Adv. Funct. Mater.* **2019**, 29, No. 1807176.
- (18) Qian, W.; Texter, J.; Yan, F. Frontiers in Poly(Ionic Liquid)s: Syntheses and Applications. *Chem. Soc. Rev.* **2017**, *46*, 1124–1159.
- (19) Wang, M.; Ford, M. J.; Zhou, C.; Seifrid, M.; Nguyen, T.-Q.; Bazan, G. C. Linear Conjugated Polymer Backbones Improve Alignment in Nanogroove-Assisted Organic Field-Effect Transistors. *J. Am. Chem. Soc.* **2017**, *139*, 17624–17631.
- (20) Wang, M.; Ford, M. J.; Lill, A. T.; Phan, H.; Nguyen, T.-Q.; Bazan, G. C. Hole Mobility and Electron Injection Properties of D-A Conjugated Copolymers with Fluorinated Phenylene Acceptor Units. *Adv. Mater* 2017, 29, No. 1603830.
- (21) Sanoja, G. E.; Schauser, N. S.; Bartels, J. M.; Evans, C. M.; Helgeson, M. E.; Seshadri, R.; Segalman, R. A. Ion Transport in Dynamic Polymer Networks Based on Metal—Ligand Coordination: Effect of Cross-Linker Concentration. *Macromolecules* **2018**, *51*, 2017—2026.
- (22) Wang, C.; Ma, X.; Kitazawa, Y.; Kobayashi, Y.; Zhang, S.; Kokubo, H.; Watanabe, M. From Macromolecular to Small-Molecular Triggers: Facile Method toward Photoinduced LCST Phase Behavior of Thermoresponsive Polymers in Mixed Ionic Liquids Containing an Azobenzene Moiety. *Macromol. Rapid Commun.* **2016**, *37*, 1960–1965.
- (23) Weis, P.; Wu, S. Light-Switchable Azobenzene-Containing Macromolecules: From UV to Near Infrared. *Macromol. Rapid Commun.* **2018**, 39, No. 1700220.
- (24) Weis, P.; Tian, W.; Wu, S. Photoinduced Liquefaction of Azobenzene-Containing Polymers. *Chem. Eur. J.* **2018**, *24*, 6494–6505.
- (25) Jangu, C.; Schultz, A. R.; Wall, C. E.; Esker, A. R.; Long, T. E. Diphenylphosphino Styrene-Containing Homopolymers: Influence of Alkylation and Mobile Anions on Physical Properties. *Macromol. Rapid Commun.* **2016**, *37*, 1212–1217.
- (26) Chen, M.; Dugger, J. W.; Li, X.; Wang, Y.; Kumar, R.; Meek, K. M.; Uhrig, D. W.; Browning, J. F.; Madsen, L. A.; Long, T. E.; Lokitz, B. S. Polymerized Ionic Liquids: Effects of Counter-Anions on Ion Conduction and Polymerization Kinetics. *J. Polym. Sci., Part A: Polym. Chem.* **2018**, *56*, 1346–1357.
- (27) Goetzberger, A.; Knobloch, J.; Voss, B. Crystalline Silicon Solar Cells; John Wiley & Sons Inc.: Chichester, 1998.
- (28) Vetráková, L'.; Ladányi, V.; Al Anshori, J.; Dvořák, P.; Wirz, J.; Heger, D. The Absorption Spectrum of Cis -Azobenzene. Photochem. Photobiol. Sci. 2017, 16, 1749–1756.
- (29) Zhou, H.; Xue, C.; Weis, P.; Suzuki, Y.; Huang, S.; Koynov, K.; Auernhammer, G. K.; Berger, R.; Butt, H.-J.; Wu, S. Photoswitching of Glass Transition Temperatures of Azobenzene-Containing Polymers Induces Reversible Solid-to-Liquid Transitions. *Nat. Chem.* **2017**, *9*, 145–151.
- (30) Yue, Y.; Norikane, Y.; Azumi, R.; Koyama, E. Light-Induced Mechanical Response in Crosslinked Liquid-Crystalline Polymers with Photoswitchable Glass Transition Temperatures. *Nat. Commun.* **2018**, *9*, No. 3234.
- (31) Kuenstler, A. S.; Clark, K. D.; Read de Alaniz, J.; Hayward, R. C. Reversible Actuation via Photoisomerization-Induced Melting of a Semicrystalline Poly(Azobenzene). *ACS Macro Lett* **2020**, *9*, 902–909.
- (32) Sze, S. M.; Ng, K. K. Physics of Semiconductor Devices, 3rd ed.; John Wiley & Sons Inc.: Hoboken, NJ, 2021.
- (33) Ho, J. C.; Arango, A.; Bulović, V. Lateral Organic Bilayer Heterojunction Photoconductors. *Appl. Phys. Lett.* **2008**, 93, No. 063305.
- (34) Nojima, H.; Kobayashi, T.; Nagase, T.; Naito, H. Modulated Photocurrent Spectroscopy for Determination of Electron and Hole Mobilities in Working Organic Solar Cells. *Sci. Rep* **2019**, *9*, No. 20346.

- (35) Maruhashi, H.; Oku, T.; Suzuki, A.; Akiyama, T.; Yamasaki, Y. In Fabrication and Characterization of P3HT:PCBM-Based Thin Film Organic Solar Cells with Zinc Phthalocyanine, AIP Conference Proceedings, American Institute of Physics: Tsukuba-city, Ibaraki, Japan, 2015; pp 89–95.
- (36) Mauer, R.; Kastler, M.; Laquai, F. The Impact of Polymer Regioregularity on Charge Transport and Efficiency of P3HT:PCBM Photovoltaic Devices. *Adv. Funct. Mater* **2010**, *20*, 2085–2092.